Sodium bicarbonate-hydroxyapatite used for removal of lead ions from aqueous solution

Silviu Adrian Predoi, Steluta Carmen Ciobanu, Carmen Mariana Chifiriuc, Simona Liliana Iconaru, Daniela Predoi, Catalin Constantin Negrila, Ioana Cristina Marinas, Steinar Raaen, Krzysztof Rokosz, Mikael Motelica-Heino

Ceramics International xxx (xxxx) xxx

Contents lists available at ScienceDirect

Ceramics International

journal homepage: www.elsevier.com/locate/ceramint

Sodium bicarbonate-hydroxyapatite used for removal of lead ions from aqueous solution

Silviu Adrian Predoi [a,b,c], Steluta Carmen Ciobanu [d], Carmen Mariana Chifiriuc [c,e,f], Simona Liliana Iconaru [d], Daniela Predoi [d,*], Catalin Constantin Negrila [d], Ioana Cristina Marinas [c], Steinar Raaen [g], Krzysztof Rokosz [h], Mikael Motelica-Heino [i]

[a] École Normale Supérieure Paris-Saclay, Département de Physique, 4 Avenue des Sciences, 91190, Gif-sur-Yvette, France
[b] Université Paris-Saclay, Physique Fondamentale, 3 rue Joliot Curie, 911190, Gif-sur-Yvette, France
[c] Life, Environmental and Earth Sciences Division, Research Institute of the University of Bucharest (ICUB), University of Bucharest, 060023, Bucharest, Romania
[d] National Institute of Materials Physics, Atomistilor Street, No. 405A, P.O. Box MG 07, 077125, Magurele, Romania
[e] Department of Microbiology, Faculty of Biology, University of Bucharest, 1-3 Aleea Portocalelor Str., District 5, 060101, Bucharest, Romania
[f] Biological Sciences Division, The Romanian Academy, 25, Calea Victoriei, 010071, Bucharest, Romania
[g] Department of Physics, Norwegian University of Science and Technology (NTNU), Realfagbygget E3-124 Høgskoleringen 5, NO 7491, Trondheim, Norway
[h] Faculty of Electronics and Computer Science, Koszalin University of Technology, Śniadeckich 2, PL 75-453 Koszalin, Poland
[i] Department of Civil Engineering and Environment, Université d'Orléans, ISTO, UMR 7327 CNRS, 1A Rue de la Férollerie, 45071, Orléans, France

ARTICLE INFO

Handling Editor: Dr P. Vincenzini

Keywords:
Nanocomposite
Non-destructive evaluation
Porosity
Lead removal
Environmental applications

ABSTRACT

This study reports the development of a novel biocomposite for potential applications in the environmental remediation. The hydroxyapatite/sodium bicarbonate (HAp-SB) biocomposite obtained by a cheap method could offer promising characteristics to be used in environmental applications. The obtaining of HAp-SB ceramic composites was studied with the aim of increasing the adsorption efficiency of lead ions from contaminated waters. A composite material (HAp-SB) with good crystallinity that preserves the hexagonal structure of pure hydroxyapatite was obtained. For the powder recovered after decontamination of the lead solution (PbHAp-SB), the XRD model highlighted additional maxima belonging to $Ca_{10}(PO_4)_5(OH)_2$, $Ca0.805Pb_{4.195}(PO_4)(OH)$ and $PbH_2P_2O_7$. The FTIR spectra of PbHAp-SB are similar to those of HAp-SB composites showing a broadening of the vibration peaks and a slight shift. The XPS and EDS studies illustrated the purity of the HAp-SB sample. Moreover, the presence of lead in the powder recovered after decontamination was also highlighted by XPS and EDS studies. The efficiency of HAp-SB in the adsorption of Pb^{2+} ions from the contaminated solution was also highlighted by ultrasound studies using double-distilled water as the reference liquid. The adsorption kinetics were investigated with the aid of Langmuir and Freundlich theoretical models. The results demonstrated that the HAp-SB ceramic composite has a strong affinity for the adsorption of Pb^{2+} ions from contaminated solutions. The removal efficiency of Pb^{2+} ions was about 92% for the initial Pb^{2+} concentration above 50 mg/L. The results of the cell viability and cytotoxicity studies demonstrated that HAp-SB nanoparticles did not influence negatively the HeLa cell's viability and did not induce any significant changes of the morphological features of HeLa cells after 24 h of incubation. The batch adsorption results as well as the cytotoxicity assay results suggested that the HAp-SB powder could be successfully used for the removal of Pb^{2+} from contaminated water.

1. Introduction

One of the toxic metals that can be found in the polluted surface or underground waters, it is represented by lead (Pb^{2+}) [1,2]. In the last years, numerous studies regarding the harmful effects of Pb against humans, including children and environment have been reported. The reported harmful effects are diverse and usually the exposure of humans to Pb is associated with toxicity to every organ system such as neurological, renal, cardiovascular, hematological, immunological, reproductive, and developmental, even at the lowest lead concentrations studied around ≤5 μg/dL. The exposure limits of lead that exhibit toxic effects on specific organ systems have not yet been identified but

* Corresponding author. National Institute of Materials Physics, Atomistilor Street, No. 405A, P.O. Box MG 07, 077125, Magurele, Romania.
E-mail address: dpredoi@gmail.com (D. Predoi).

https://doi.org/10.1016/j.ceramint.2023.10.273
Received 26 August 2023; Received in revised form 19 October 2023; Accepted 25 October 2023
Available online 28 October 2023

extensive information regarding the effects of lead ions in human populations, environment and in experimental animals are available [3–10]. However, because the lowest lead concentrations are associated with serious adverse effects so far the MRLs for lead have not been derived. Lead is a non-biodegradable element that can severely affect the central nervous system. Studies have reported that lead could be responsible for neurological deficits in children, and that could affect the IQ by 3–4 points for each 10 μg Pb/dL increase in the blood levels of children. In this context, in 1993, WHO proposed an amended guideline value for lead in drinking water of 10 μg Pb/L. In 2008, WHO confirmed the guideline value for lead in drinking water (10 μg/L). The accumulation in the human body of lead and/or others pollutants may lead to cause serious health problems. In the study conducted by Al-Weher et al. [11] was showed that exposure of aquatic organism (fish) to heavy metals increased their mortality risks. In this context, as a solution, the researchers proposed the use of nanomaterials based on calcium phosphates in the depollution process of waters contaminated with heavy metals [12–15]. Hydroxyapatite (HAp, Ca/P ratio equal to 1.67.),[1] is a well-known biomaterial and is the main inorganic component of the calcified tissues [16]. Furthermore, besides the special biological properties, HAp possesses good adsorption properties. The good capability of hydroxyapatite to adsorb heavy metals and other pollutants from the aqueous media have been previously reported [17,18]. As shown previously, HAp may be developed by various methods (routes) like wet precipitation, solid-state reaction, hydro/solvothermal, sol-gel, emulsion methods, etc. [19]. A relatively facile and cheap method that can be successfully used to develop hydroxyapatite nanopowders is coprecipitation [20].

In this context, calcium phosphate materials together with others swelling and ordinary clays were proposed as cheap and accessible adsorbent materials. An eco-friendly and simply to use method used for the decontamination of polluted aqueous solution is represented by adsorption [21]. Another well-known and effective method used in the environment pollution management; it is represented by ion-exchange method [14]. Due to the unique plasticity of the HAp structure that allow a large number of substitutions and even the presence of vacancies, the substitution can take place in the anionic or in the cationic sites [14] of the hydroxyapatite structure.

The results reported by Rogina et al. [22], in their work entitled "Cellular hydrogels based on pH-responsive chitosan-hydroxyapatite system" showed that the presence of sodium bicarbonate in the synthesis process of the chitosan-hydroxyapatite system allow the obtaining of a hydrogel with potential uses as cell carrier. On the other hand, Fabbri et al. [23] studied the development of polycaprolactone/hydroxyapatite (PCL/HAp)[2] composites by sol gel route, using sodium bicarbonate as porogen agent. Their results suggest that through the method proposed by them, porous materials with good biocompatibility and which sustain the proliferation of preosteoblastic cells can be obtained [23]. Moreover, the presence of heavy metals such as cadmium (Cd) strontium (Sr), lead (Pb) has been shown that may induce high toxicity against HeLa cells [24–26]. Thus, Doi et al. [27] investigated the biocompatibility of calcium phosphate cements using HeLa and osteoclast cell line and their findings suggest that the studied samples possess good biocompatibility features [27].

Therefore, in this paper we report for the first time our findings regarding the obtaining of a new biocomposite powder based on hydroxyapatite coated with sodium bicarbonate (HAp-SB)[3] with potential application in environmental remediation. The new powders were obtained by a coprecipitation method. Different characterization techniques were involved to study the new nanoparticles before and after the lead decontamination experiments and together corroborate to identify their unique physicochemical and biological characteristics. To the best of our knowledge, to date there is a lack of published work describing the functionalization of hydroxyapatite with sodium bicarbonate for environmental applications. Even fewer of them have addressed the complex study of physicochemical properties (structural, morphological, compositional, porosity, batch adsorption and ultrasonic studies) along with biological ones. Using the synthesis method proposed in this paper, new inexpensive materials with desired characteristics, good lead adsorption capacity and good biocompatibility can be obtained. This study aims at developing a novel material with biocompatible properties that can also be used for water remediation. Often, the use of nanoparticles in the environmental remediation could affect the ecosystem and pose a risk to human health. Therefore, the objective of this study was to obtain a biocompatible material with low toxicity that could be used for water treatment. In this context, the study presents both results regarding the toxicity of the HAp_SB nanoparticles as well as results regarding their efficiency in removing lead ions from contaminated water.

2. Materials and methods

2.1. Materials

To obtain the powder used in the present study, ammonium dihydrogen phosphate [$(NH_4)_2HPO_4$], calcium nitrate [$Ca(NO_3)_2{\cdot}4H_2O$], sodium bicarbonate ($NaHCO_3$) purchased from Sigma Aldrich Corporation with ≥99% purity were used. Lead nitrate [$Pb(NO_3)_2$] with 99.999% purity was purchased from Sigma Aldrich Corporation, too. Extra pure HCl solution acquired from Merck. Double distilled water was used throughout the experiment.

2.2. Preparation of sodium bicarbonate-hydroxyapatite

$(NH_4)_2HPO_4$ and $Ca(NO_3)_2.4H_2O$ solutions were prepared in agreement with previous research [28]. $NaHCO_3$ (10 g) was added to the $(NH_4)_2HPO_4$ solution and stirred at 40 °C for 30 min. The molar ratio of Ca/P was 1.67. The $Ca(NO_3)_2.4H_2O$ solution was added into the solution of $NaHCO_3$ and $(NH_4)_2HPO_4$ and stirred at 40 °C for 4 h. The pH was maintained at 8.5–9.0. The resulting precipitate was washed thoroughly (five times). At the end, the product resulting from the centrifugation was dried at 100 °C. The powder obtained after drying (HAp-SB) was analyzed and used in the decontamination experiments.

2.3. Physico-chemical characterizations

Afterward, a comprehensive analysis (from a physico-chemical and biological point of view) of the powders was carried out both before and after the adsorption experiments. Techniques such as X-ray diffraction (XRD),[4] scanning electron microscopy (SEM),[5] energy dispersive X-ray (EDX),[6] Fourier transform infrared spectroscopy (FTIR),[7] N_2 adsorption-desorption studies (by BET method),[8] X-ray photoelectron spectroscopy (XPS)[9] and ultrasound studies were used to get valuable information about the studied powders. Furthermore, the sorption of lead ions from aqueous solutions using HAp-SB nanoparticles was evaluated by adsorption batch experiments. The biocompatibility of the new materials was evaluated using the HeLa cell line. The structural features of sodium bicarbonate-hydroxyapatite were investigated by X-ray diffraction (XRD) studies. The XRD measurements were made with a Bruker D8

[1] Hydroxyapatite: HAp.
[2] polycaprolactone/hydroxyapatite: PCL/HAp.
[3] Hydroxyapatite coated with sodium bicarbonate: HAp-SB.
[4] X-ray diffraction: XRD.
[5] Scanning electron microscopy: SEM.
[6] Energy dispersive X-ray spectroscopy: EDX.
[7] Fourier transform infrared spectroscopy: FTIR.
[8] BET method: Brunauer, Emmett and Teller method.
[9] X-ray photoelectron spectroscopy: XPS.

Advance diffractometer (Bruker, Karlsruhe, Germany) instrument. The measurements were recorded using a nickel filtered $Cu_{K\alpha}$ ($\lambda = 1.5418$ Å) radiation and a high-efficiency one-dimensional detector (Lynx Eye type) operated in integration mode. The XRD diffractograms were obtained for the 2θ range 10°–70°, using 34 s measuring time per step and a step of 0.02°. A Hitachi S4500 scanning electron microscope was employed for the studies regarding the morphology and chemical composition of HAp-SB powder (before and after the decontamination experiments).

The Fourier-transform infrared spectroscopy (FTIR) technique was used in order to evidence the vibrational bands present in the HAp-SB powder (before and after the decontamination experiments). For this purpose, a Perkin Elmer SP-100 spectrometer (Waltham, MS, USA) operated in attenuated total reflection mode was used. The FTIR spectra were recorded between 450 and 2000 cm^{-1}. The procedure used for the obtaining of the second derivative spectra was described in detail in Ref. [29]. The X-ray photoelectron spectroscopy (XPS) spectra were recorded using the following parameters: energy window of 20 eV; resolution R = 20 eV and 400 recording channels. The obtained XPS spectra were processed with Spectral Data Processor v2.3 (SDP) software. The N_2 adsorption-desorption measurements were made with the aid of a Micromeritics ASAP 2020 Physisorption Analyzer (Micromeritics Instrument Corp., Norcross, GA, USA). The sample of lead-contaminated water (100 ml of suspension) and the sample of water after lead removal (100 ml of suspension) were poured into a special transparent cubical container to be analyzed. Two coaxial ultrasonic transducers are immersed in the suspension and are distanced by 16 mm face-to-face. The transducers' axis is at 29 mm from the flat bottom of the container box. The samples were continuously stirred for 10 min at 500 rot/min in order to obtain a good homogeneity of the solid particles before being analyzed. Immediately after stopping the magnetic stirring machine, began the acquisition of the 1000 ultrasonic signals, recorded every 5s from the oscilloscope. Each signal is an average of 32 successive signals, in order to eliminate the possible electric noise.

2.4. Batch adsorption experiments

The retention of Pb^{2+} from contaminated water was evaluated with the aid of batch adsorption experiments. The experiments were performed according to the protocol described in Ref. [26]. All the batch adsorption experiments were performed in silicon tubes. The Pb^{2+} concentrations from the contaminated water were in the range of 0–100 mg/L. For the batch adsorption experiments, 0.2 g of HAp-SB nanoparticles were used. The contaminated water with 0.2 g of HAp-SB nanoparticles was stirred for 24 h at room temperature. Meanwhile, the volume of the mixture for each tube was 20 mL. The pH value was monitored and kept stable at 6 during the experiment. After 24 h, the samples were centrifuged for 1 h, at 10000 rpm. Afterward, the supernatant was filtered and analyzed by Flame Atomic Absorption Spectrometry (AAS)[10] with the aid of a Zeeman HITACHI Z-8100 instrument. The wavelength used for the measurements was the one at 283.3 nm prevued by the operational conditions for lead. Furthermore, the theoretical models developed by Langmuir and Freundlich [30,31] were used in order to obtain information regarding the mechanisms involved in the adsorption of Pb^{2+} onto HAp-SB nanoparticles. For this purpose, the amount of the adsorbed metal ions onto the HAp-SB nanoparticles at the equilibrium, Q_e (mg/g), was derived using the following Langmuir equation, $Q_e = \frac{(C_o - C_e)}{m} \cdot V$. More than that, information about the adsorption process was determined by calculating the values of the Langmuir constants, q_m and K_L using the linear form of the Langmuir equation, $\frac{C_e}{Q_e} = \frac{1}{(q_m \bullet K_L)} + \frac{C_e}{q_m}$ [30]. In addition, complementary information about the adsorption of Pb^{2+} onto HAp-SB nanoparticles was also derived from the Freundlich model, $Q_e = k_f \bullet C_e^{\frac{1}{n}}$. For this purpose, the linear form of the Freundlich equation $ln\, Q_e = ln\, k_f + \frac{1}{n} ln\, C_e$ [1] was employed for the determination of Freundlich parameters, adsorption capacity (k_f) and the adsorption intensity of the adsorbent (n).

2.5. In vitro biological studies

The biocompatibility studies of the HAp-SB nanoparticles were done *in vitro* using the MTT (3-4,5-Dimethylthiazol 2,5-diphenyltetrazolium bromide)[11] assay. The studies were performed as previously described in Refs. [32,33], using HeLa cells. The cell viability was assessed after a period of incubation of 24 h. The biocompatibility studies were performed for HAp-SB nanoparticles and also for the contaminated aqueous solutions before and after the decontamination experiments. The HeLa cell viability was determined using a TECAN spectrophotometer (Tecan GENios, Grödic, Germany) instrument by quantifying the absorbance of the suspensions at a wavelength of 595 nm. The MTT studies were performed in triplicate and the results were presented as mean ± SD (standard deviation). In addition, optical microscopy was used to study any changes that could have occurred in the morphology of the HeLa cells after being incubated for 24 h with HAp-SB nanoparticles and with the contaminated and decontaminated solutions.

3. Results and discussions

The XRD pattern of HAp-SB powder before and after decontamination are depicted in Fig. 1. Fig. 1a exhibits the XRD pattern of HAp-SB before decontamination and the standard pattern of pure hydroxyapatite JCPDS no. 09-0432.[12] The peaks of the XRD pattern of sample HAp-SB (Fig. 1a) correspond to those of pure hexagonal HAp and space group P63/m. The XRD pattern of the HAp-SB powder indicated a good crystallinity of the structure. This fact is revealed by the sharp peaks that appear in the XRD pattern of HAp-SB. The XRD pattern of the powder recovered after decontamination (PbHAp-SB)[13] is presented in Fig. 1b. The reflection peaks of the XRD spectrum of PbHAp-SB were slightly shifted to higher diffraction angles compared to HAp-SB. Besides the maxima belonging to hexagonal HAp, the XRD pattern of PbHAp-SB highlighted the presence of additional peaks. The additional peaks were identified as belonging to calcium lead phosphate hydroxide (JCPDS no. 010-3163) and lead hydrogen phosphate (JCPDS no. 012-0005). Reference models for $Ca_{10}(PO_4)_5(OH)_2$ (JCPDS no. 09-0432), $Ca_{0.805}Pb_{4.195}(PO_4)(OH)$ (JCPDS no 010-3163) and $PbH_2P_2O_7$ (JCPDS no. 012-0005) were also presented in Fig. 1c–e.

In addition, a noticeable decrease of the peaks associated with HAp can be observed in the XRD spectrum of PbHAp-SB, while the peaks associated with $Ca_{0.805}Pb_{4.195}(PO_4)(OH)$ and $PbH_2P_2O_7$ appeared. This behavior suggests the existence of ion exchange in Pb^{2+} adsorption by HAp-SB. The obtained results are in good agreement with previous reported data [34] which showed that Ca^{2+} ions replaced Pb^{2+} ions from the environment (contaminated solution). This result highlights the fact that HAp-SB powder has a high potential for removing pollutants from contaminated waters.

In Fig. 2, the XPS survey spectra of the HAp-SB composite were presented before (Fig. 2a) and after it was used in the process of removing lead ions from the contaminated solution (Fig. 2b). The XPS survey spectrum of HAp-SB (Fig. XPS_a) shows the binding energies of C 1s, O 1s, Ca 2p, P 2p and Na 1s. The XPS survey spectrum recorded after the adsorption of lead ions (PbHAp-SB) also highlights the binding

[10] Flame Atomic Absorption Spectrometry: AAS.

[11] (3-4,5-Dimethylthiazol 2,5-diphenyltetrazolium bromide) assay: MTT assay.

[12] Joint Committee on Powder Diffraction Standards: JCPDS.

[13] HAp-SB powder recovered after decontamination: PbHAp-SB.

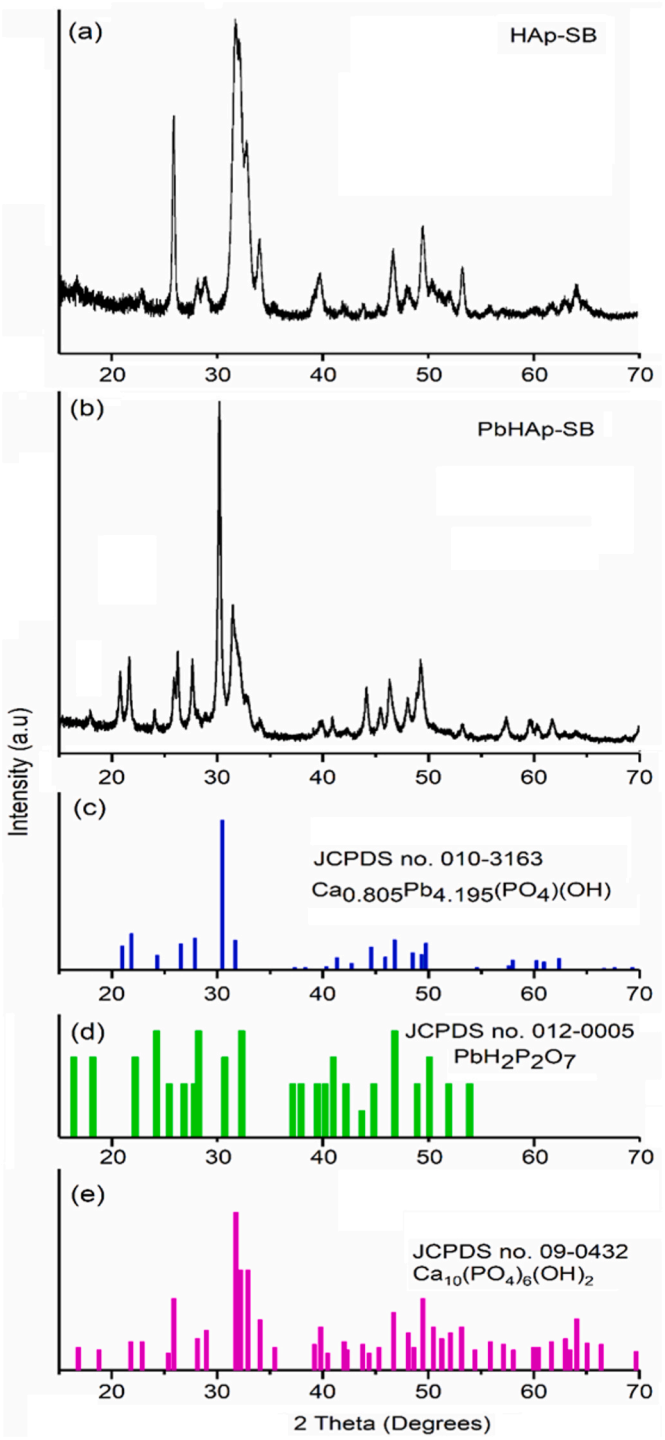

Fig. 1. (**a**): XRD patterns of the HAp-SB; (**b**): XRD patterns of the PbHAp-SB; (**c**) $Ca_{0.805}Pb_{4.195}(PO_4)(OH)$ (JCPDS no 010-3163); (**d**) $PbH_2P_2O_7$ (JCPDS n. 012-0005); (**e**) $Ca_{10}(PO_4)_5(OH)_2$ (JCPDS no. 09-0432).

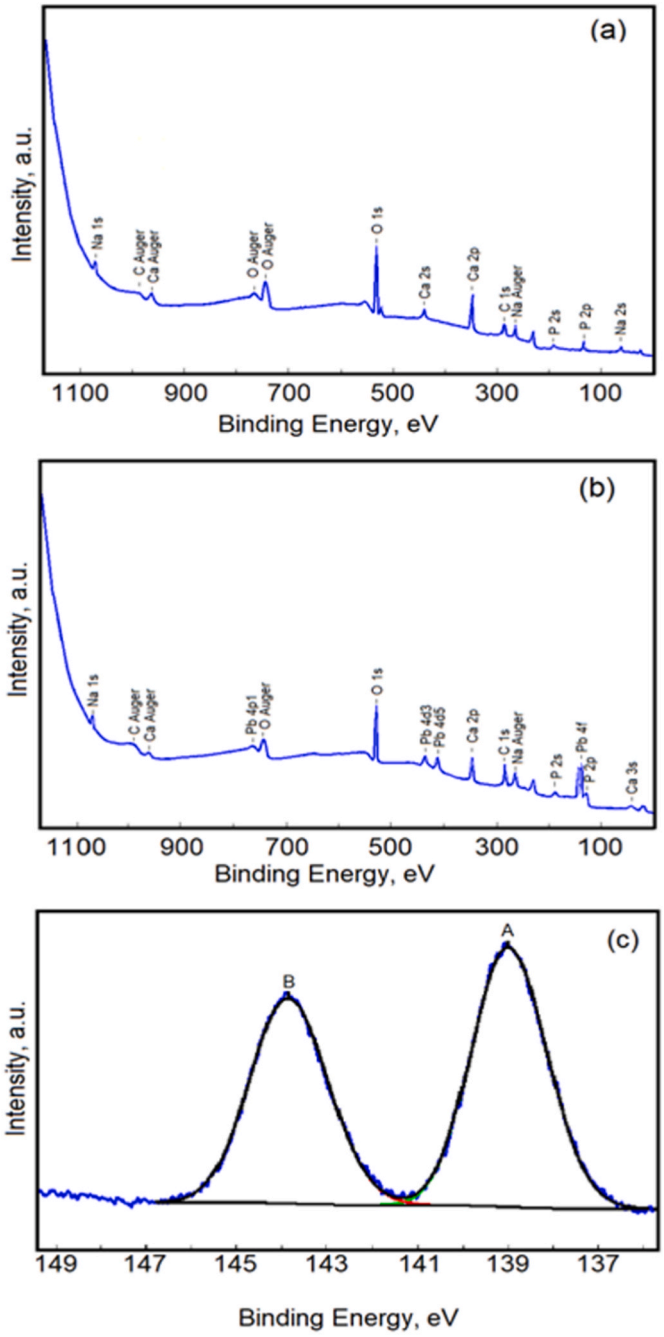

Fig. 2. XPS survey spectra of HAp-SB (**a**), and PbHAp-SB(**b**). High resolution spectra of Pb 4f (**c**).

energy of Pb 4f (Fig. 2b). In Fig. 2c the high-resolution XPS spectrum of Pb 4f is presented. Peaks A and B at 138.99 eV and 143.86 eV, respectively, were assigned to Pb $4f^{7/2}$ and Pb $4f^{5/2}$. The distance between the two maxima is approximately 4.8 eV with an area ratio of 4:3. The binding energy is higher than that of ordinary oxides, which indicates that most of the lead ions enter the hydroxyapatite network. This result is in full accord with the XRD studies.

The morphology of HAp-SB and PbHAp-SB samples was evaluated using Scanning Electron Microscopy (SEM) technique (Fig. 3a and b). As it can be observed from both SEM micrographs, the morphology of the powders (before lead decontamination experiments) they consist mainly of nanometrically sized particles with an almost spherical morphology.

In the case of PbHAp-SB nanopowders, the particles exhibit an almost ellipsoidal morphology, preserving their nanometric dimension. Also, the formation of a new phase it is suggested by the presence of particles with a plate-like morphology. Moreover, in Fig. 3a and b can be noticed the high tendency of nanoparticles to agglomerate. Therefore, the results of the scanning electron microscopy studies reveal that after the lead decontamination experiments, the morphology of the PbHAp-SB recovered nanopowder it is slightly changed compared to the HAp-SB nanopowder morphology.

The experimental data obtained by EDX analysis mainly consist of spectra that are highlighting the presence of peaks corresponding to the

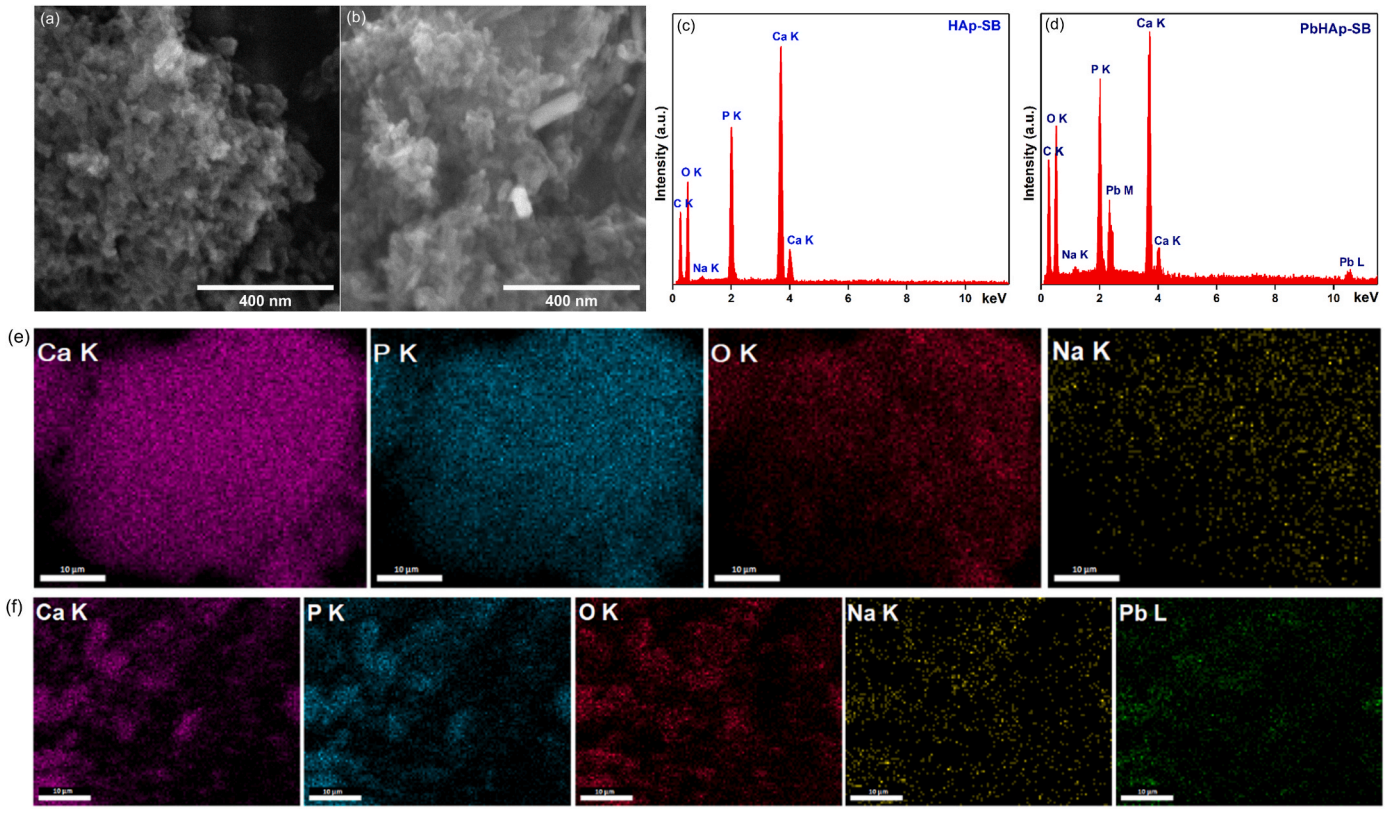

Fig. 3. 2D Scanning electron microscopy micrographs of HAp-SB (**a**) and PbHAp-SB (**b**) samples; EDX spectra obtained for the HAp-SB (**c**) and PbHAp-SB powders (**d**) and elemental cartographies of the HAp-SB powders (e) and PbHAp-SB powders (f).

elements that are making up the composition of the studied materials. Therefore, in Fig. 3 c,d are presented the EDX spectra that are obtained on the HAp-SB sample before (Fig. 3c) and after (Fig. 3d) lead decontamination experiments. In the both EDX spectra can be noticed the presence of the Ca, P and O peaks, that are arising due to the presence of hydroxyapatite in the studied materials. Furthermore, the presence of the Na line was observed in both spectra and their occurrence it is mainly due to the sodium bicarbonate that was used in the synthesis process. For the powders recovered after de lead decontamination experiments (PbHAp-SB), in the EDX spectra, appear the Pb (M and L) lines which confirms the good adsorption of Pb^{2+} by the HAp-SB samples. As it can be seen in Fig. 3c and d no supplementary peaks can be noticed, which shows the purity of the analyzed nanomaterials.

Additional information regarding the chemical composition of the HAp-SB and PbHAp-SB powders were obtained by elemental cartography and the results are depicted in Fig. 3e and f. For the HAp-SB sample, studied before the lead decontamination experiments, the main obtained cartographies belong to the Ca, P, O and Na, that are the chemical elements that are found in the HAp-SB composition (Fig. 3e). On the other hand, for the PbHAp-SB powders recovered and analyzed after the lead decontamination experiments, in addition to the specific cartographies of the chemical elements found in the structure of the HAb-Sb sample, a specific cartography of adsorbed Pb was also obtained (Fig. 3f). Likewise, could be observed in all the obtained cartographies, a high homogeneity and a well distribution of these chemical elements in the studied nanopowders.

The FTIR measurements were used in order to put in evidence the functional groups present in both HAp-SB and PbHAp-SB nanopowders and their results are revealed in Fig. 4a,c. In Fig. 4a are presented the typical FTIR spectra of HAp-SB nanopowder. The obtained FTIR spectra highlight the presence of the main peaks which belong to the vibration of phosphate and hydroxyl groups from the hydroxyapatite structure. The presence of the phosphate group in the HAp-SB sample is clearly proved by the maxima that are observed at 474 cm^{-1}, 561 cm^{-1}, 601 cm^{-1}, 632 cm^{-1}, 961 cm^{-1},1025 cm^{-1}, and 1089 cm^{-1} [35–37]. Furthermore, the peak from 872 cm^{-1} may be attributed to the HPO_4^{2-} group vibration in HAp structure [36]. Meanwhile, according to the studies conducted by Slosarczyk et al. [37] the maxima founded at around 870 cm^{-1} are specific to the ν_2 vibration of carbonate groups. Finally, the broad maxima that are found between 1400 and 1450 cm^{-1} are characteristics to B-type carbonate (ν_3 CO_3^{2-}) vibration [35,37].

It was observed that the FTIR spectra obtained for the powders recovered after lead decontamination experiments (PbHAp-SB), is quite similar to the FTIR spectra of the initial powders (HAp-SB). However, a slight displacement and a broadening of the vibrational peaks can be noticed. In Table 1 are summarized the main peaks assignments and their position, for the obtained HAp-SB nanopowders.

For a better accuracy, the FTIR second derivative spectra of HAp-SB and PbHAp-SB samples in the ν_3, ν_2, ν_4 and ν_1 phosphate peaks are shown in Fig. 4b, d. In the second derivative spectra of HAp-SB powders could be observed the presence of the maxima at around 961 cm^{-1} which is characteristic to the ν_1 molecular vibration of the phosphate groups in the HAp structure. Also, was identified a broad peak at around 474 cm^{-1} which can be assigned to ν_2 molecular vibration of the phosphate groups. More than that, between 500 cm^{-1} and 700 cm^{-1} are found bands that belong to ν_4 phosphate vibration. In the 900–1200 cm^{-1} spectral domain can be identified the maxima that are characteristic to ν_1 and ν_3 molecular vibration of phosphate groups. Furthermore, the very broad band observed at around 873 cm^{-1} are related to the presence of the ν_2 vibration of carbonate groups in the studied materials. The second derivative spectra obtained for the PbHAp-SB, suggest a decrease of the vibrational band intensity which may indicate a decrease in the crystallinity degree of the samples. The findings of our FTIR

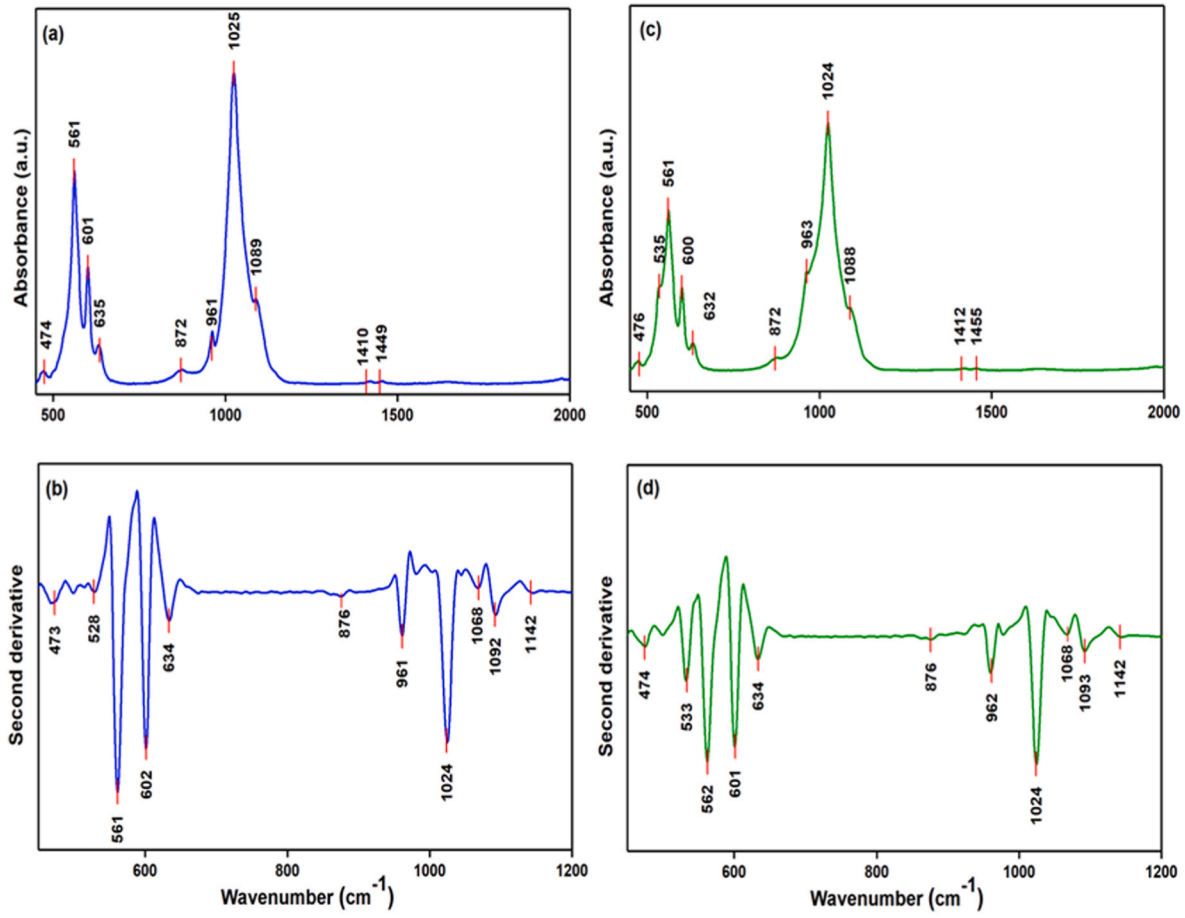

Fig. 4. FTIR spectra characteristic for the HAp-SB (**a**) and PbHAp-SB (**c**) samples. Second derivative spectra obtained for the HAp-SB (**b**) and PbHAp-SB (**d**) samples.

Table 1
The IR vibrational peaks position for the HAp-SB nanopowders.

Peak assignments	IR vibrational peaks position (cm^{-1})
ν_1 phosphate	961
ν_2 phosphate	474
ν_3 phosphate	1025, 1089
ν_4 phosphate	561, 601, 635
ν_2 carbonate	873
ν_3 carbonate	1400–1450

studies are in good accord with the results reported by Sroka-Bartnicka et al. [38] in their work entitled "Structural transformation of synthetic hydroxyapatite under simulated *in vivo* conditions studied with ATR-FTIR[14] spectroscopic imaging".

Fig. 5a showed the N_2 adsorption-desorption isotherm of HAp-SB. The adsorption isotherm was of the type IV, showing an H3 hysteresis loop curve according to IUPAC[15] [39]. According to previous studies [40], the H3 hysteresis loop revealed that the existing pores in HAp-SB were in the form of the wedge and/or slit shaped. According to the studies conducted on "adsorption properties" [41], type IV adsorption isotherms come from capillary condensation after multilayer adsorption in mesopores. Since the H3 hysteresis loop does not have a plateau at high P/P0 values, Rouquerol et al. [42] considered that this type IV hysteresis form could be a pseudo-type II. They associate this behavior (a pseudo-type II) with metastability of the adsorbed multilayer and

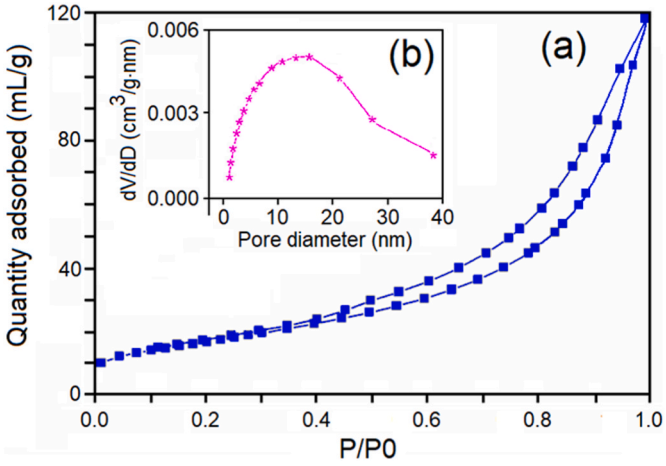

Fig. 5. The N_2 adsorption-desorption isotherms of the synthetized HAp-SB (**a**) and pore size distribution (**b**).

delayed capillary condensation. Moreover, Rouquerol et al. [42] considered that the shape of the H3 loop is related to the nature of the adsorbent. The pore size distribution revealed that the pores were mainly mesoporous. The pore size distributions of HAp-SB presented in Fig. 8b were calculated with the Barret–Joyner–Halenda (BJH)[16] model from their desorption data. The average pore diameter and total

[14] Attenuated total reflectance: ATR.
[15] International Union of Pure and Applied Chemistry: IUPAC.
[16] Barret–Joyner–Halenda model: BJH.

pore volume of HAp-SB sample were 12.24 nm 0.23 cm^3/g, respectively. The Brunauer-Emmett-Teller (BET) surface area of HAp-SB sample was 72.34 cm^2/g.

The adsorption capacity of HAp-SB nanoparticles of Pb^{2+} from contaminated water was investigated using the flame atomic absorption spectroscopy (AAS) technique. The experiments were performed in triplicate in normal atmospheric conditions.

The efficiency of HAp-SB in retaining $Pb^{2+}$from contaminated water was determined using an initial pH between range 2–7. The studies were performed using a contaminated solution having a concentration of Pb^{2+} equal to 50 mg/L. The results highlighted that the capacity of HAp-SB in the removal of Pb^{2+}considerably increased when the value of the pH was raised from 2 to 4 and afterward it remained constant from 4.5 to 6. These results were in compliance with the literature [43–45]. There have been reported several possible reactions responsible for the removal of Pb^{2+} from contaminated solutions [43–46]. One possible mechanism has been depicted as the adsorption of Pb^{2+} on the HAp surface. This was reported to be quickly followed by a reaction of ion exchange between Pb^{2+} and Ca^{2+} from the HAp lattice. The ion exchange reactions could be described as:

$$Pb^{2+}_{(a)} + \equiv Ca^{2+}_{(b)} \rightarrow \equiv Pb^{2+}_{(b)} + Ca^{2+}_{(a)} \quad (R1)$$

in which, the subscripts (a) and (b) describe the solution and the hydroxyapatite phase. The reaction describes that the metal ion from the solution (Pb^{2+}(a)) replaces a surface ion, (Ca^{2+}) of the sorbent ($\equiv Ca^{2+}$(b)).

Furthermore, a possible second mechanism that was reported in this case was the one of surface complexation. The possible reactions involved correlated with the pH value variation were identified as the following:

$$\equiv CaOH_2^+ \leftrightarrow \equiv CaOH^0 + H^+ \quad (R2)$$

$$\equiv PO^- + H^+ \leftrightarrow POH^0 \quad (R3)$$

In their studies regarding the "Removal of lead (II) from aqueous solutions using carbonate hydroxyapatite extracted from eggshell waste" Liao et al. [46] reported that the poor Pb^{2+} removal could be attributed to the fact that for a low pH value, the existing H^+ causes an increase of the $CaOH_2^+$ and POH^0 populations that led to a net positive charge. A net positive charge is less favorable for the complexation of Pb^{2+} on the HAp surface than a net negative charge.

Therefore, in this work, the pH value of 6 was considered to be the most favorable pH value to carry out the adsorption batch experiments and to determine the HAp-SB capacity of adsorption of lead ions from contaminated water.

The capacity of HAp-SB nanoparticles in removing of Pb^{2+} ions from contaminated water was obtained using the results of the batch adsorption experiments and is depicted in Fig. 6 a. Fig. 6a presents the graphical representation of the percentage of removal efficiency (R%) function of the initial Pb^{2+}concentration from the contaminated solutions. The results highlighted that the value of R% regarding removal of Pb^{2+}using HAp-SB nanoparticles was above 88%. Furthermore, the results also indicated that the R% value was influenced by the initial Pb^{2+}

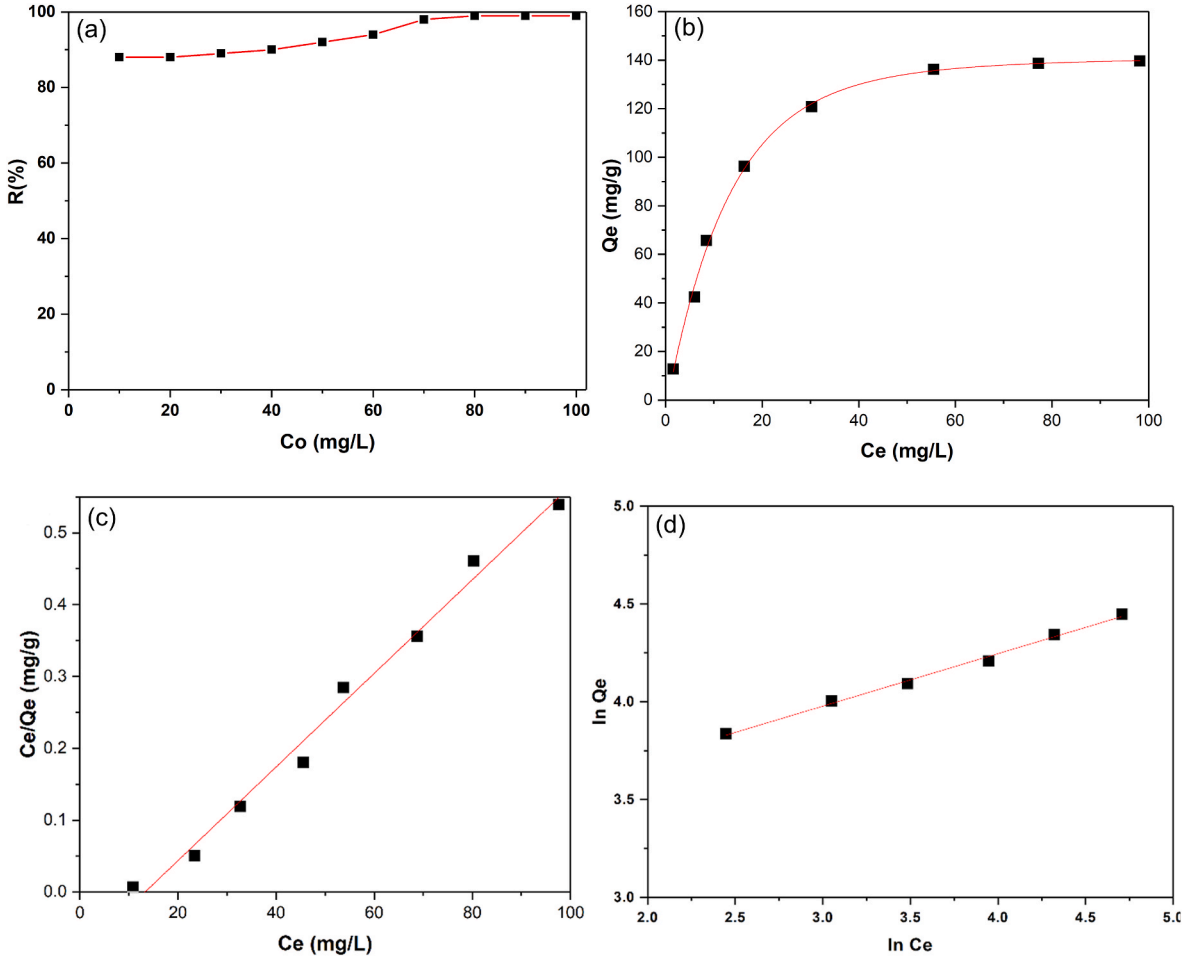

Fig. 6. The removal percentage of Pb^{2+} ions from contaminated aqueous solutions using HAp-SB nanoparticles (a); Graphical representation of the amount of Pb^{2+} ions adsorbed at equilibrium by HAp-SB nanoparticles (b) and Langmuir (**c**) and Freundlich (**d**) linear graphical representation of the equations for the adsorption of Pb^{2+} ions on HAp-SB nanoparticles.

concentration of the contaminated solution. The results attained for the removal efficiency (R%) emphasized that HAp-SB nanoparticles exhibited a strong affinity towards Pb^{2+} ions displaying a removal efficiency (R%) of approximately 92% when the initial Pb^{2+} concentration was over 50 mg/L.

Information about the mechanism involved in the adsorption processes of lead ions using HAp-SB nanoparticles were illustrated with the aid of Langmuir and Freundlich adsorption models [47,48]. Langmuir theoretic adsorption model was elaborated at first for the representation of activated carbon gas-solid adsorption. Afterward, the Langmuir theoretical model of adsorption was employed for the determination of adsorption efficiency of numerous materials [49]. The theoretical adsorption model elaborated by Langmuir define the theory in the case of a monolayer adsorption process and details an adsorption process specific to a finite and localized number of well-defined areas, that are identical and equivalent [49,50]. The fitting of the experimental data using the Langmuir model for the Pb^{2+} adsorption from contaminated water with the aid of HAp-SB nanoparticles is represented in Fig. 6b.

The results gathered about the capability of HAp-SB nanoparticles in the removal of Pb^{2+} from contaminated water highlighted that HAp-SB nanoparticles exhibited a high affinity towards Pb^{2+} ions. The results obtained by fitting the data from the batch experiments showed that both for Langmuir and Freundlich isotherm models the obtained R^2 values were equal or above 0.99. This fact suggested that both models were a good fit for the adsorption of Pb^{2+} onto HAp-SB nanoparticles. On the other hand, the results, highlighted that the Langmuir model ($R^2 = 0.995$) better fitted the experimental data resulting from the batch adsorption experiments compared to the Freundlich model ($R^2 = 0.994$). The adsorption kinetic parameters were also calculated using the linear form of the equations obtained for the adsorption of Pb^{2+} on HAp-SB nanoparticles, which are depicted in Fig. 6 c,d.

The Langmuir constants, adsorption capacity (q_m) and equilibrium characteristic constant of the adsorbent (K_L), determined from the AAS experimental data following the Langmuir adsorption model disclosed a value of 153.37 ± 4.14 mg (Pb)/g for q_m and a value of 0.081 L/mg for the K_L coefficient. Furthermore, the Freundlich model was also used to better apprehend the mechanisms responsible for the removal of Pb^{2+} ions from contaminated water by HAp-SB nanoparticles. Freundlich equation was first described by Herbert Freundlich in 1909 [51,52]. The theoretical model proposed by Herbert Freundlich depicts an empirical correlation among the adsorbed gas on the surface of the adsorbent and the value of the pressure. It could be used to describe the surface heterogeneity of adsorbents and give an exponential distribution of active sites and their energies. According to the model, the value of 1/n quantified from the Freundlich equation illustrates the linearity of adsorption or the degree of curvature of the isotherms for the tested concentrations of contaminant metal ions. The Freundlich adsorption model states that if the Freundlich constant, n, has a value equal to 1, it represents that the separation of the two phases does not depend on the concentration, and signifies that the adsorption partition of the chemical has been the same for all the tested concentrations (C-type isotherm). Often, the values of 1/n could be found in the interval 0.7–1.0. The values of 1/n depict that when the concentration of the metal ion that is investigated increases, the relative adsorption shows a decrease that corresponds to a L-type isotherm. These values indicate the saturation of adsorption sites available to the metal ion, resulting in a relatively low adsorption, while the 1/n values below 0.7 express highly curved isotherms. The 1/n values that are above 1 correspond to S-type isotherms. These types of isotherms are not commonly encountered but it has been reported to be often observed for low concentration ranges in the case of samples that have in their composition a polar functional group. This behavior was hypothesized to be attributed to the fact that, when at low concentrations, the compounds are in competition with the water molecules for the available adsorption sites [53]. The values that were calculated from the experimental data for the Langmuir and Freundlich parameters are presented in Table 2.

Table 2
Langmuir and Freundlich isotherm parameters for Pb^{2+} adsorption onto HAp-SB nanoparticles.

Sample	Langmuir			Freundlich		
HAp-SB	R^2	q_m (mg/g)	K_L (L/mg)	R^2	n	k_f
	0.995	153.37 ± 4.14	0.081	0.994	3.73	23.81

The results obtained by fitting the experimental data using Freundlich isotherm model highlighted that the value for n which was calculated from the linearized Freundlich equation in the case of Pb^{2+} ions adsorption onto HAp-SB nanoparticles, was higher than 1. The results displayed the value of 1/n being lower than 1, which suggests a normal adsorption process in the case of lead ions adsorption on HAp-SB nanoparticles. The analysis of the data gathered from the batch adsorption experiments determined that the Langmuir isotherm model described better the adsorption of Pb^{2+} ions on the HAp-SB nanoparticles from aqueous solution as indicated by the high correlation coefficient (R^2) of 0.995. More than that, the calculated value of R_L was between 0 and 1, which indicates a favorable adsorption process for the presented experimental conditions. The Langmuir monolayer adsorption capacity (q_m) value was found to be 153.37 mg/g indicating that the HAp-SB nanoparticles possess a high adsorption capacity for the Pb^{2+}. In addition, the value of K_L (0.081 L/mg) determined from the linearized Langmuir equation was relatively high suggesting a high surface energy in the process and therefore a high bonding between the metal ions and the HAp-SB nanoparticles. It was also observed that the Freundlich isotherm conformed to the experimental data having a correlation coefficient value, $R^2 = 0.994$. The R^2 value obtained from the linearized Freundlich model for HAp-SB nanoparticles implies having a multilayer structure in the adsorption process. This result is in agreement with gas adsorption-desorption studies that highlighted a multi-layer adsorption.

The calculated n value was equal to 3.73 which indicated that the HAp-SB exhibited a heterogeneous surface satisfying the heterogeneity condition, $1 < n < 10$. The determined value of 1/n was below one, indicating a chemisorption process, while the value of k_f was found to be 23.81, which indicated that there was a high uptake of Pb^{2+} on the adsorbents surface.

In agreement with previous studies [54], the multilayer adsorption is the rule rather than the exception and the development of models is very difficult because a second layer cannot be seen without the adsorbent-adsorbate interaction. Rigorous theories are difficult to develop. A generally accepted model is that proposed by Brunauer, Emmett and Teller, commonly known as the BET theory [55]. Regarding multilayer adsorption, the BET model assumes approximately the same position as that of Langmuir. Thus, it was considered that the adsorption is localized, the surface is homogeneous and the lateral interaction is ignored.

Moreover, the data highlighted that the adsorption of Pb^{2+} on HAp nanoparticles in normal atmospheric conditions and at pH 6 was high, as a result of the large between Pb^{2+} and HAp-SB nanoparticles. These results could be attributed to the fact that Pb^{2+} can be adsorbed on the surface of the hydroxyapatite through the substitution of Ca^{2+} with Pb^{2+} [56–58]. Over the years, a few possible reactions in the case of the removal of lead from contaminated water have been proposed. The most often encountered were reported to be surface adsorption, ion exchange or substitution, and precipitation [59]. Even though there have been numerous studies in this area and results regarding the role of phosphate minerals such as apatite, modified apatite and/or hydroxyapatite-based composites in controlling the behavior of lead ions concentrations in soils [60] or in contaminated wastewater [61–65], the actual mechanisms involved in these processes are still poorly understood. In their studies about “Formation and stability of base metal phosphates in soils and sediments”, Nriagu et al. [66] proposed that this process involves a two-step reaction that is constituted by the sorption of lead on metal oxides, and of a subsequent reaction of the orthophosphate ions from the

solution that lead to the formation of lead phosphate as a solid. Until the present day, one of the most detailed reports regarding the use of calcium apatite in lead ions removal are those performed by Suzuki et al. [63–65] that proposed that lead ions from the contaminated solution substitutes the calcium ions from the apatite structure on 1:1 basis. More recent studies conducted by Iconaru et al. [36] reported that the main mechanism in the adsorption of lead ions by hydroxyapatite nanoparticles was determined by the partial dissolution of the hydroxyapatite followed by the pyromorphite reprecipitation. Similar results have been reported by Xu et al. [67] the involved reaction mechanisms of the lead ions adsorption process onto hydroxyapatite were the dissolution of hydroxyapatite powders followed by the precipitation of lead apatite. Meanwhile, based on the substitution model proposed by Suzuki et al. [65], Takeuchi and Arai [68] proposed that the process involved in the removal of lead ions from contaminated water could be controlled kinetically with the aid of a liquid-film diffusion of Pb^{2+} and Ca^{2+} near the surface of HAp grains. Furthermore, McLean and Bledsoe [69] emphasized that the precipitation vs. the surface sorption could be influenced by the concentration of the metal ions. Their study also implied that the relevance of precipitation vs. surface sorption is correlated with both the metal ions concentrations and also with the amounts and activities of the surface sites [69]. The results obtained in our present study from the batch adsorption experiments as well as the combined results on solution and solid-phase physico-chemical analyses undoubtedly established that Pb^{2+} were removed from the contaminated water and that they precipitated in various forms of lead apatite minerals. Furthermore, the results obtained from the batch experiments and the data determined with the aid of the theoretical models developed by Langmuir and Freundlich suggested that HAp-SB nanoparticles had a strong affinity for the adsorption of Pb^{2+} ions from contaminated solutions. These results highlighted that HAp-SB nanoparticles could be excellent candidates for future advancement in the area of water remediation technologies.

The ultrasound studies were carried out both on water contaminated with lead and on the water obtained after the removal of lead. The recorded signals. A direct image of the recorded signals is shown on Fig. 7a–b. From right to left are plotted as waterflow all 1000 signals covering 5000 s of process evolution. It is visible a rapid change of signals amplitudes and time delays. A more visible evolution is shown in Fig. 7c–d. Regarding the contaminated water, the initial signal is very weak, but increases to an amplitude close to that in the reference liquid (double distilled water) $A/A_{ref} = 1$ after 120 s. The process is not uniform and for about 10 min, the maximal amplitude oscillates around the relative unit value. This evolution can be explained by the formation of clusters which in some conditions settle faster than the remaining particles in suspension. During the initial 120 s, the ultrasonic waves exhibit an increase in velocity from 1491.5 m/s to 1494.8 m/s. The velocity is increasing for higher suspension average bulk modulus and diminishes

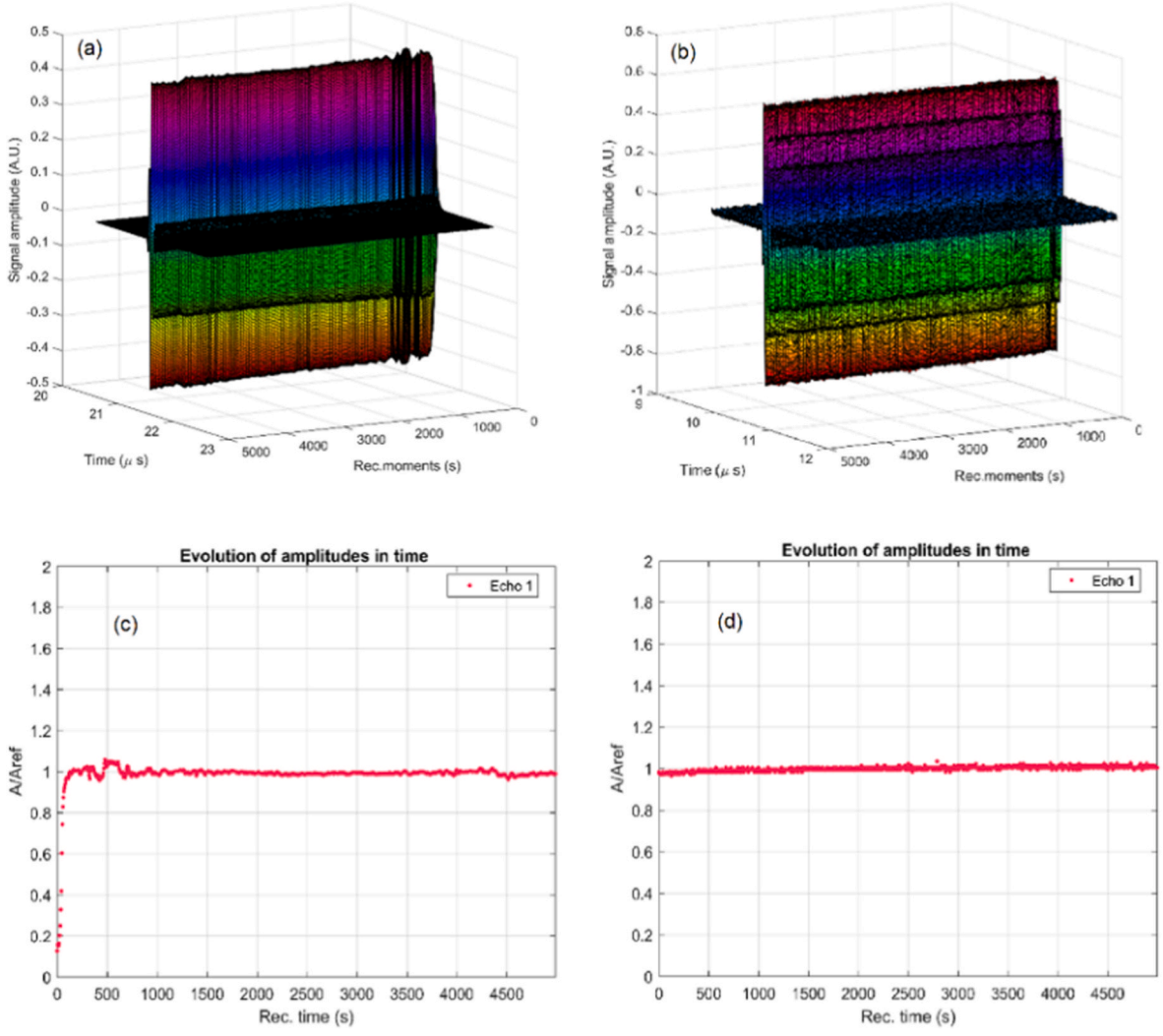

Fig. 7. Time evolution of the recorded signals, from left to right over 5000 s for contaminated (a) and decontaminated (**b**) water. Recorded signals amplitudes during the experiment for contaminated (**c**) and decontaminated (**d**) water.

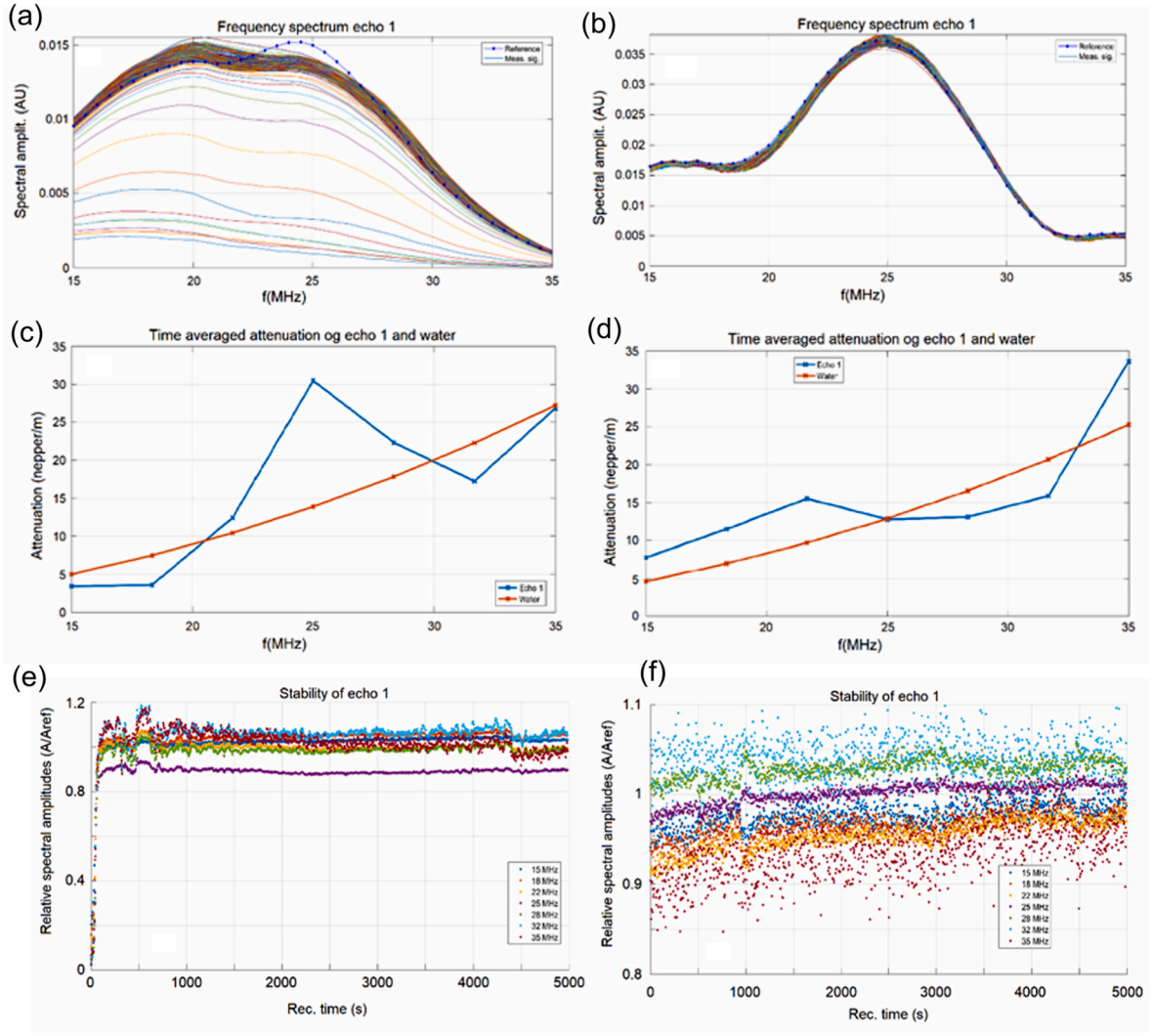

Fig. 8. Spectral amplitudes of all 1000 signals for contaminated (**a**) and decontaminated (**b**) water. Time averaged attenuation for the investigated frequency range for contaminated (**c**) and decontaminated (**d**) water and the relative spectral amplitudes vs. time for contaminated (e) and decontaminated (f) water.

with the average mass density. One can attribute the measured evolution to a reduction of the average mass density as the larger solid particles are sedimented. In the case of decontaminated water, a very slow increase in the amplitude of the measured signal was observed, which indicated a slow sedimentation of the particles remaining in suspension.

The frequency spectra of all the signals recorded for contaminated and decontaminated water are shown in Fig. 8a–d. For comparison is also plotted the spectrum of the same signal, but through the reference liquid (in dotted blue line). For contaminated water, the initial rapid evolution is represented by the weak amplitudes spectra at the lower part of Fig. 8. As the suspension becomes stable, the spectra are approaching that of distilled water, but with significant differences. At frequencies which lower than the central frequency of the transducers (24.5 MHz as obtained for the measured signal in the reference liquid), the amplitudes are clearly higher in the contaminated water sample. This remark is valid also for higher frequencies. Only in the interval 23.5–27 MHz the amplitudes in the contaminated water sample are lower than those in the reference liquid. This proves a higher attenuation of the suspension in this frequency range, proven by the time averaged attenuation plot shown on Fig. 8c. Compared against the standard attenuation in the reference liquid (red dotted line) the attenuation is considerably larger for the contaminated water sample. At 25 MHz the attenuation surpasses 30 nepper/m whereas for water it is only 14 nepper/m.

The slow evolution of signals for the decontaminated water sample is represented by the concentration of the 1000 spectral curves near the spectrum of the reference liquid (double-distilled water). At frequencies which lower than the central frequency of the transducers (24.5 MHz as obtained for the measured signal in the reference liquid), the amplitudes are slightly lower in the decontaminated water sample. Above the central frequency, the spectra are much tighter, indicating a close resemblance to the reference liquid. The time averaged attenuation plot is shown on Fig. 8d. Compared against the standard attenuation in the reference liquid (red dotted line) the attenuation is slightly larger for the decontaminated water sample in the lower and higher frequency ranges. In the frequency range 25–32 MHz, the attenuation is below the attenuation in the reference liquid, indicating some residual nanoparticles in suspension.

Another contaminated water suspension characteristic is the spectral stability, representing the amplitude of the frequency component of each spectrum, as function of time (Fig. 8e). During the initial period of 10 min spectral amplitudes have irregular evolutions due to cluster formation and sedimentation, for every plotted frequency. The weaker amplitude at 25 MHz remains stable up to the end of the experiment, but all the others present a sudden reduction after 4400 s. This reduction can be attributed to a loss of stability of the suspended nanoparticles, some being settled on the transducers. The tips of the transducers are of conical frustum shape and it is possible that some accumulated particles

fell in front of the ultrasonic beam. The contaminated water sample becomes stable after 10 min, when the majority of larger particles and clusters of particles have settled on the bottom of the container. The signal amplitude has then a small variation and the stability parameter S $= 4.76e^{-05}$. The spectral stability of decontaminated water was presented in Fig. 8f. All spectral amplitudes are slowly increasing in time, in the order of 5%. After about 1000 s of monitoring, a perturbation in the spectral evolution occurred. The lower frequencies (15-22 MHz) have a temporary decrease of amplitude, whereas the higher frequencies are of temporary increased amplitude. This process of short duration (~200s) process can be associated to the formation of clusters of nanoparticles, which settle more rapidly passing in front of the transducers. The decontaminated water sample is relatively stable, the stability parameter $S = \frac{\overline{dA}}{Adt} = 1.6e^{-05}$, in which A is the signal amplitude, with a bar above indicating averaging. This is relatively stable sample with average properties close to those of the reference liquid. The stability becomes very good after about 1 h of monitoring.

The biocompatibility of HAp-SB nanoparticles (Fig. 9) as well as the cytotoxicity of the HAp-SB nanoparticles (Fig. 9) used in the removal of Pb^{2+} from contaminated water were investigated using HeLa cell line. To achieve this, the cytotoxicity of HAp-SB nanoparticles as well as lead-contaminated solution and decontaminated solutions using HAp-SB nanoparticles was studied. During the biological assays, HeLa cells were incubated for 24 h with HAp-SB nanoparticles, lead-contaminated

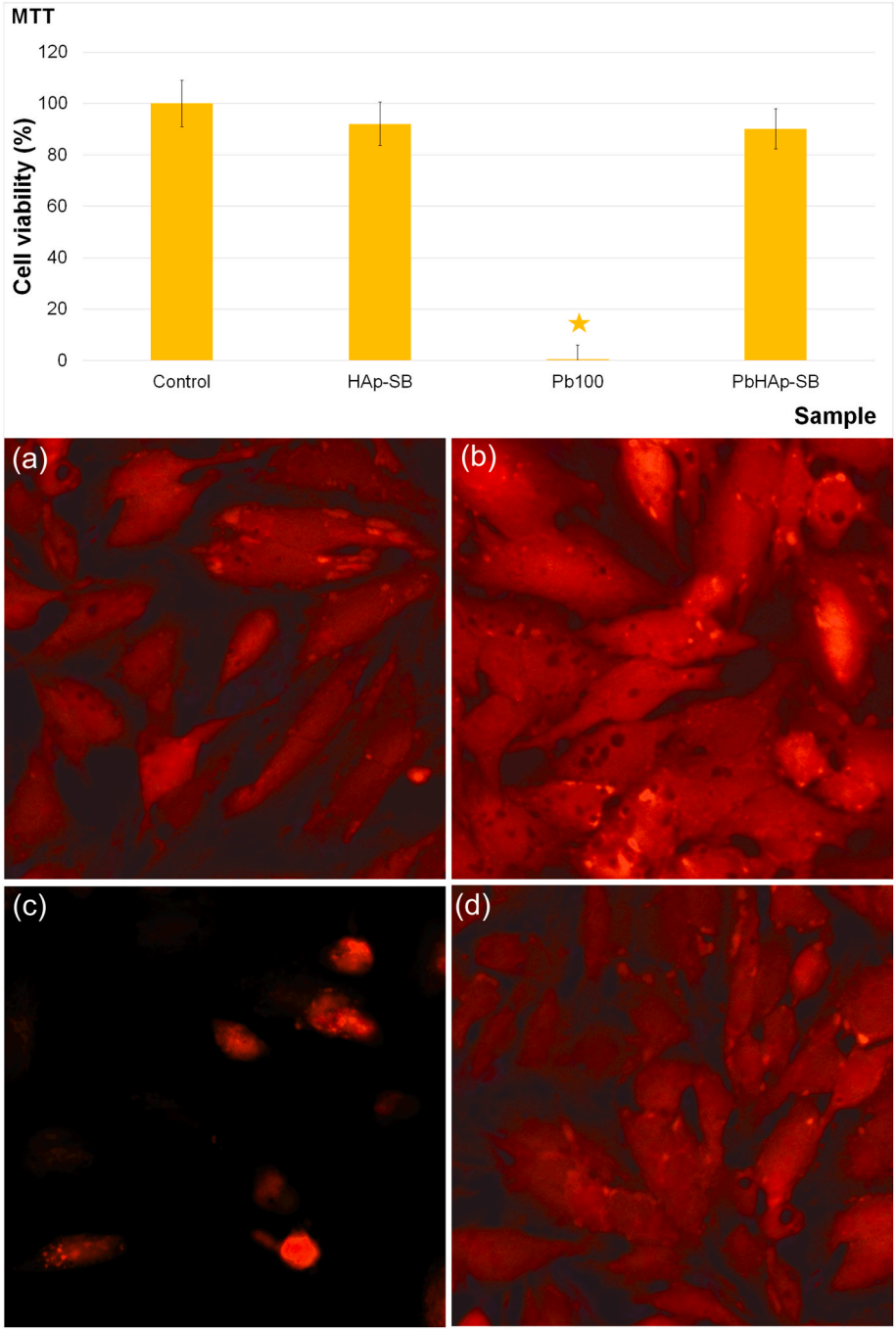

Fig. 9. MTT assay of the cell viability of HeLa cells incubated with HAp-SB nanoparticles, Pb^{2+} contaminated solution, and decontaminated solution using HAp-SB nanoparticles. A HeLa free cell culture was used as control and the optical visualization of the morphology of the HeLa cells used as control (a); incubated with HAp-SB nanoparticles (b), incubated with Pb^{2+} contaminated solutions (c), and incubated with solutions decontaminated using HAp-SB nanoparticles (d).

solution having a Pb^{2+} concentration of 100 mg/L, (Pb100),[17] and also with the decontaminated solution using HAp-SB nanoparticles (PbHAp-SB) and their viability was investigated by MTT assay. The results of the MTT biological studies, showing the viability of the HeLa after a 24 h incubation with HAp-SB nanoparticles, lead-contaminated solutions and with the decontaminated solutions using HAp-SB nanoparticles are depicted in Fig. 9.

The MTT studies showed that HAp-SB nanoparticles did not display a significant toxicity on the HeLa cells viability while the lead-contaminated solution presented strong harmful effects towards HeLa cells after 24 h of contact. Furthermore, the results evidenced that the HeLa cell viability decreased to a value below 1% after being incubated with the Pb100 solution. The MTT assays conducted on the aqueous decontaminated solutions using HAp-SB nanoparticles are also presented in Fig. 9. The data emphasized that the decontaminated solution did not induce any significant effects on the rate of the HeLa culture's cell viability after 24 h of incubation. More than that, the MTT results demonstrated that in the case of the decontaminated solution, the cell viability was approximately 90%. The cell viability values resulting from the MTT studies highlighted that HAp-SB nanoparticles could be considered in the development of novel materials with good biocompatible properties. In addition, the data also suggested that these types of materials could be successfully used in for the removal of Pb^{2+} from contaminated water. Lead is well known for being a naturally occurring element that is non-biodegradable and possesses great toxicity [70–72]. The toxicity of lead and its harmful effects on different types of organs like the nervous system, the red blood cells, the hematopoietic system, the endocrine system, the reproductive system, and kidneys, was reported for even small concentrations [70–72].

Complementary information about the biological properties of HAp-SB nanoparticles and lead-contaminated and decontaminated solutions was obtained by evaluating the morphology of HeLa cells after 24 h of incubation with the samples by microscopic visualization. The HeLa cell's morphology after 24 h of exposure to HAp-SB nanoparticles, lead-contaminated solutions at a concentration of 100 mg/L and with decontaminated solutions using HAp-SB nanoparticles are presented in Fig. 9 a-d. The optical microscopic observation of the morphological changes that occurred in HeLa cells after 24 h of contact with the investigated samples were in good agreement with the data obtained from the quantitative MTT studies and suggested that HAp-SB nanoparticles did not provoke any significant morphological changes in the HeLa cells after 24 of incubation. The optical observation emphasized that the HeLa cell's morphological features were not visible modified after being exposed for 24 h to the decontaminated solution using HAp-SB nanoparticles. On the other hand, the images obtained with the aid of the optical microscopy depicted that the morphological features of the HeLa cells exposed that were exposed to the lead-contaminated aqueous solution were fundamentally changed indicating that the presence of lead ions exhibited a considerable toxic effect on the HeLa cells after 24 h of incubation. More than that, the microscopic images showed that the HeLa cells incubated with the lead-contaminated solutions exhibited a distinctive apoptotic appearance and a considerable cell number reduction. The results obtained from the visual observation of the cells are in concordance with the results of the MTT studies and with previously reported studies that reported the harmful effects and high toxicity of lead ions [70–78]. The preliminary results obtained in this study regarding the biocompatibility of HAp-SB nanoparticles as well as the promising data obtained in the case of the removal of Pb^{2+} from aqueous solutions using HAp-SB nanoparticles determined that these nanoparticles could be suitable in the future development of novel environmental remediation technologies.

[17] Lead-contaminated solution having a Pb^{2+} concentration of 100 mg/L: Pb100 solution.

4. Conclusions

This study was aimed on the recovery of Pb^{2+} ions from the contaminated aqueous solution using a new composite based on hydroxyapatite coated with sodium bicarbonate (HAp-SB) obtained by co-precipitation. The results of XRD studies reveal that the HAp-SB before decontamination preserves the hexagonal structure with lattice parameters characteristic to pure hydroxyapatite. After lead ions removal, the peaks of the XRD spectrum of the resulting powder (PbHAp-SB) were slightly shifted to higher diffraction angles compared to HAp-SB, and additional peaks were identified. EDS and XPS spectra of powder after lead removal highlighted the presence of lead. Furthermore, the experimental results of the XPS and EDS studies underline the purity of the analyzed samples. The efficiency HAp-SB nanoparticles in the removal of lead ions was determined using the data obtained from the batch adsorption experiments and ultrasound measurements. The results of the FTIR studies reveal the presence of the principal peaks that belongs to the molecular vibration of the phosphate groups in the HAp structure. Moreover, the results of the MTT studies showed that HAp-SB nanoparticles have the potential to be considered in the development of new materials with improved biocompatible properties that may be successfully used in the removal of lead ions from contaminated solutions. All the results obtained in this study show that the HAp-SB powder obtained by the co-precipitation method is effective for removing Pb^{2+} ions from the contaminated solution.

Data availability

The datasets generated during and/or analyzed during the current study are available from the corresponding author on reasonable request.

Declaration of competing interest

The authors declare that they have no known competing financial interests or personal relationships that could have appeared to influence the work reported in this paper.

Acknowledgements

This work is funded by the Core Program of the National Institute of Materials Physics, granted by the Romanian Ministry of Research, Innovation and Digitalization through the Project PC1– PN23080101 and by the Project to Support Institutional Excellence contract 35PFE/2022 (funded by the Romanian Ministry of Research, Innovation and Digitization).

References

[1] Y. Zhu, Z. Zhu, X. Zhao, Y. Liang, Y. Huang, Characterization, dissolution, and solubility of lead hydroxypyromorphite [Pb5 (PO4) 3OH] at 25–45 C, J. Chem. 2015 (2015) 1–11, https://doi.org/10.1155/2015/269387.

[2] S. Paul, A. Mandal, P. Bhattacharjee, S. Chakraborty, R. Paul, B.K. Mukhopadhyay, Evaluation of water quality and toxicity after exposure of lead nitrate in fresh water fish, major source of water pollution, Egypt J. Aquat. Res. 45 (2019) 345–351, https://doi.org/10.1016/j.ejar.2019.09.001.

[3] ATSDR, Agency for Toxic Substances & Disease Registry: Toxicological Profile for Lead, U.S. Department of Health and Human Services, Atlanta, 2007.

[4] EFSA, EFSA panel on contaminants in the food chain (CONTAM); scientific opinion on lead in food, EFSA J. 8 (1570) (2010) 1147. Available online: http://www.efsa.europa.eu/en/efsajournal/pub/1570.htm.

[5] IPCS, Safety Evaluation of Certain Food Additives and Contaminants: Lead, 2000. WHO Food Additives Series, Prepared by the Fifty-third meeting of the Joint FAO/WHO Expert Committee on Food Additives (JECFA). Available online: http://www.inchem.org/documents/jecfa/jecmono/v44jec12.htm 44.

[6] VRAR, Voluntary Risk Assessment Report on Lead and Some Inorganic Lead Compounds – Human Health Section, 2008. Report prepared by ILZRO and EBRC Consulting under contract to the LDAI Lead Risk Assessment Working Group, http://www.chem.unep.ch/Pb_and_Cd/SR/GOV/VRAR_Pb_0707_hh.pdf.

[7] H.L. Wang, X.T. Chen, B. Yang, F.L. Ma, S. Wang, M.L. Tang, M.G. Hao, D.Y. Ruan, Case-control study of blood lead levels and attention deficit hyperactivity disorder in Chinese children, Environ. Health Perspect. 116 (2008) 1401–1406.
[8] WHO, Lead in Drinking Water. Background Document for Preparation of WHO Guidelines for Drinking- Water Quality, 2003. World Health Organization (WHO/SDE/WSH/03.04), Geneva.
[9] WHO, Principles for Evaluating Health Risks in Children Associated with Exposure to Chemicals in Environmental Health Criteria No. 237, World Health Organization – IPCS International Program on Chemical Safety, Geneva, 2006.
[10] WHO, Guidelines for Drinking-Water Quality, Vol. 1, third ed., 2008 incorporating 1st and 2nd addenda.
[11] S.M. Al-Weher, Levels of heavy metal Cd, Cu and Zn in three fish species collected from the Northern Jordan Valley, Jordan, J. Biol. Sci. 1 (2008) 41–46.
[12] A. Corami, S. Mignardi, V. Ferrini, Copper and zinc decontamination from single- and binary-metal solutions using hydroxyapatite, J. Hazard Mater. 146 (2007) 164–170, https://doi.org/10.1016/j.jhazmat.2006.12.003.
[13] Y. Zheng, J. Zhang, Experimental study on the adsorption of dissolved heavy metals by nano-hydroxyapatite, Water Sci. Technol. 82 (2020) 1825–1832, https://doi.org/10.2166/wst.2020.465.
[14] M. Ibrahim, M. Labaki, J.M. Giraudon, J.F. Lamonier, Hydroxyapatite, a multifunctional material for air, water and soil pollution control: a review, J. Hazard Mater. 383 (2020), 121139, https://doi.org/10.1016/j.jhazmat.2019.121139.
[15] M. Ferri, S. Campisi, M. Scavini, C. Evangelisti, P. Carniti, A. Gervasini, In-depth study of the mechanism of heavy metal trapping on the surface of hydroxyapatite, Appl. Surf. Sci. 475 (2019) 397–409, https://doi.org/10.1016/j.apsusc.2018.12.264.
[16] S.C. Doca, G.A. Vlase, T.I. Vlase, A.T. Galuscan, O.C. Balean, D.A. Negru, D. Jumanca, The use of bisphosphonate-hydroxyapatite composite in bone augmentation, Rev. Chim. 71 (2020) 22–30, https://doi.org/10.37358/RC.20.6.8166.
[17] Y. Feng, J.L. Gong, G.M. Zeng, Q.Y. Niu, H.Y. Zhang, C.G. Niu, J.H. Deng, M. Yan, Adsorption of Cd (II) and Zn (II) from aqueous solutions using magnetic hydroxyapatite nanoparticles as adsorbents, Chem. Eng. J. 162 (2010) 487–494, https://doi.org/10.1016/j.cej.2010.05.049.
[18] A.I. Adeogun, R.B. Babu, One-step synthesized calcium phosphate-based material for the removal of alizarin S dye from aqueous solutions: isothermal, kinetics, and thermodynamics studies, Appl. Nanosci. 11 (2015) 1–3, https://doi.org/10.1007/s13204-015-0484-9.
[19] S. Li, Y. Li, W. Shen, Y. Bai, L. Kong, Hydroxyapatite-based catalysis in environmental decontamination, J. Clean. Prod. 380 (2022), 134961, https://doi.org/10.1016/j.jclepro.2022.134961.
[20] Y. Guesmi, H. Agougui, R. Lafi, M. Jabli, A. Hafiane, Synthesis of hydroxyapatite-sodium alginate via a co-precipitation technique for efficient adsorption of Methylene Blue dye, J. Mol. Liq. 249 (2018) 912–920, https://doi.org/10.1016/j.molliq.2017.11.113.
[21] S. Swamiappan, S. Ganesan, V. Sekar, S. Devaraj, A. Subramanian, V. K. Ponnusamy, P. Kathirvel, Effective removal of cationic methylene blue dye using nano-hydroxyapatite synthesized from fish scale bio-waste, Int. J. Appl. Ceram. Technol. 18 (2021) 902–912, https://doi.org/10.1111/ijac.13672.
[22] A. Rogina, A. Ressler, I. Matić, G.G. Ferrer, I. Marijanović, M. Ivanković, H. Ivanković, Cellular hydrogels based on pH-responsive chitosan-hydroxyapatite system, Carbohydr. Polym. 166 (2017) 173–182, https://doi.org/10.1016/j.carbpol.2017.02.105.
[23] P. Fabbri, F. Bondioli, M. Messori, C. Bartoli, D. Dinucci, F. Chiellini, Porous scaffolds of polycaprolactone reinforced with in situ generated hydroxyapatite for bone tissue engineering, J. Mater. Sci. Mater. Med. 21 (2010) 343–351, https://doi.org/10.1007/s10856-009-3839-5.
[24] M.S. Samuel, E. Selvarajan, K. Subramaniam, T. Mathimani, S. Seethappan, A. Pugazhendhi, Synthesized β-cyclodextrin modified graphene oxide (β-CD-GO) composite for adsorption of cadmium and their toxicity profile in cervical cancer (HeLa) cell lines, Process Biochem. 93 (2020) 28–35, https://doi.org/10.1016/j.procbio.2020.02.014.
[25] S.A. Predoi, S.C. Ciobanu, M.C. Chifiriuc, M. Motelica-Heino, D. Predoi, S. L. Iconaru, Hydroxyapatite nanopowders for effective removal of strontium ions from aqueous solutions, Materials 16 (2023) 229, https://doi.org/10.3390/ma16010229.
[26] S.A. Predoi, C.S. Ciobanu, M. Motelica-Heino, M.C. Chifiriuc, M.L. Badea, S. L. Iconaru, Preparation of porous hydroxyapatite using cetyl trimethyl ammonium bromide as surfactant for the removal of lead ions from aquatic solutions, Polymers 13 (2021) 1617, https://doi.org/10.3390/polym13101617.
[27] Y. Doi, Y. Shimizu, Y. Moriwaki, M. Aga, H. Iwanaga, T. Shibutani, K. Yamamoto, Y. Iwayama, Development of a new calcium phosphate cement that contains sodium calcium phosphate, Biomaterials 22 (2001) 847–954, https://doi.org/10.1016/s0142-9612(00)00248-9.
[28] C.S. Ciobanu, S.L. Iconaru, F. Massuyeau, L.V. Constantin, A. Costescu, D. Predoi, Synthesis, structure, and luminescent properties of europium-doped hydroxyapatite nanocrystalline powders, J. Nanomater. 2012 (2012) 1–10, https://doi.org/10.1155/2012/942801.
[29] S.L. Iconaru, M. Motelica-Heino, D. Predoi, Study on europium-doped hydroxyapatite nanoparticles by fourier transform infrared spectroscopy and their antimicrobial properties, J. Spectros. 2013 (2013) 1–11, https://doi.org/10.1155/2013/284285.
[30] I. Langmuir, The adsorption of gases on plane surfaces of glass, mica and platinum, J. Am. Chem. Soc. 40 (1918) 1361–1403, https://doi.org/10.1021/ja02242a004.
[31] H.M.F. Freundlich, Over the adsorption in solution, J. Phys. Chem. 57 (1906) 385–471.
[32] D. Predoi, R.A. Vatasescu-Balcan, Osteoblast interaction with iron oxide nanoparticles coated with dextrin in cell culture, J. Optoelectron. Adv. Mater. 10 (2008) 152–157.
[33] A.M. Prodan, S.L. Iconaru, C.M. Chifiriuc, C. Bleotu, C.S. Ciobanu, M. Motelica-Heino, S. Sizaret, D. Predoi, Magnetic prop erties and biological activity evaluation of iron oxide nanoparticles, J. Nanomater. 2013 (2013), 893970, https://doi.org/10.1155/2013/893970.
[34] Y. Zhu, B. Huang, Z. Zhu, H. Liu, Y. Huang, X. Zhao, M. Liang, Characterization, dissolution and solubility of the hydroxypyromorphite-hydroxyapatite solid solution [(PbxCa1 x)5(PO4)3OH] at 25 degrees C and pH 2–9, Geochem. Trans. 17 (2016) 1–8, https://doi.org/10.1186/s12932-016-0034-8.
[35] R.V. Ghita, S.L. Iconaru, C.L. Popa, A. Costescu, P. le Coustumer, M. Motelica-Heino, C.S. Ciobanu, Tetraethyl orthosilicate coated hydroxyapatite powders for lead ions removal from aqueous solutions, J. Nanomater. 2014 (2014) 1–8, https://doi.org/10.1155/2014/176426.
[36] S.L. Iconaru, M. Motelica-Heino, R. Guegan, M. Beuran, A. Costescu, D. Predoi, Adsorption of Pb (II) ions onto hydroxyapatite nanopowders in aqueous solutions, Materials 11 (2018) 2204, https://doi.org/10.3390/ma11112204.
[37] A. Ślósarczyk, Z. Paszkiewicz, C. Paluszkiewicz, FTIR and XRD evaluation of carbonated hydroxyapatite powders synthesized by wet methods, J. Mol. Struct. 744 (2005) 657–661, https://doi.org/10.1016/j.molstruc.2004.11.078.
[38] A. Sroka-Bartnicka, L. Borkowski, G. Ginalska, A. Ślósarczyk, S.G. Kazarian, Structural transformation of synthetic hydroxyapatite under simulated in vivo conditions studied with ATR-FTIR spectroscopic imaging, Spectrochim. Acta Mol. Biomol. Spectrosc. 171 (2017) 155–161, https://doi.org/10.1016/j.saa.2016.07.051.
[39] H. Jiang, X. Li, L. Tian, T. Wang, Q. Wang, P. Niu, P. Chen, X. Luo, Defluoridation investigation of Yttrium by laminated Y-Zr-Al tri-metal nanocomposite and analysis of the fluoride sorption mechanism, Sci. Total Environ. 648 (2019) 1342–1353, https://doi.org/10.1016/j.scitotenv.2018.08.258.
[40] J. Xiao, R. Hu, G. Chen, Micro-nano-engineered nitrogenous bone biochar developed with a ball-milling technique for high-efficiency removal of aquatic Cd (II), Cu (II) and Pb (II), J. Hazard Mater. 387 (2020), 121980, https://doi.org/10.1016/j.jhazmat.2019.121980.
[41] Y. Hattori, K. Kaneko, T. Ohba, 5.02 - Adsorption Properties, Editor(s): Jan Reedijk, Kenneth Poeppelmeier, Comprehensive Inorganic Chemistry II, second ed., Elsevier, 2013, pp. 25–44, https://doi.org/10.1016/B978-0-08-097774-4.00502-7. ISBN 9780080965291.
[42] F. Rouquerol, J. Rouquerol, K. Sing, Adsorption by Powders and Porous Solids, Academic Press, London, 1999.
[43] S.H. Hasan, P. Srivastava, M. Talat, Biosorption of lead using immobilized Aeromonas hydrophila biomass in up flow column system: factorial design for process optimization, J. Hazard Mater. 177 (2010) 312–322, https://doi.org/10.1016/j.jhazmat.2009.12.034.
[44] L. Wu, W. Forsling, P.W. Schindler, Surface complexation of calcium minerals in aqueous solution: 1. Surface protonation at fluorapatite—water interfaces, J. Colloid Interface Sci. 147 (1991) 178–185, https://doi.org/10.1016/0021-9797(91)90145-X.
[45] S.M. Mousa, N.S. Ammar, H.A. Ibrahim, Removal of lead ions using hydroxyapatite nano-material prepared from phosphogypsum waste, J. Saudi Chem. Soc. 20 (2016) 357–365, https://doi.org/10.1016/j.jscs.2014.12.006.
[46] D. Liao, W. Zheng, X. Li, Q. Yang, X. Yue, L. Guo, G. Zeng, Removal of lead (II) from aqueous solutions using carbonate hydroxyapatite extracted from eggshell waste, J. Hazard Mater. 177 (2010) 126–130, https://doi.org/10.1016/j.jhazmat.2009.12.005.
[47] S.J. Allen, G. Mckay, J.F. Porter, Adsorption isotherm models for basic dye adsorption by peat in single and binary component systems, J. Colloid Interface Sci. 280 (2004) 322–333, https://doi.org/10.1016/j.jcis.2004.08.078.
[48] N. Ayawei, A.N. Ebelegi, D. Wankasi, Modelling and interpretation of adsorption isotherms, J. Chem. 2017 (2017) 1–11, https://doi.org/10.1155/2017/3039817.
[49] I. Langmuir, The constitution and fundamental properties of solids and liquids, J. Am. Chem. Soc. 38 (1916) 2221–2295, https://doi.org/10.1021/ja02268a002.
[50] K. Vijayaraghavan, T.V. Padmesh, K. Palanivelu, M. Velan, Biosorption of nickel (II) ions onto Sargassum wightii: application of two-parameter and three-parameter isotherm models, J. Hazard Mater. 133 (2006) 304–308, https://doi.org/10.1016/j.jhazmat.2005.10.016.
[51] H.M.F. Freundlich, Kapillarchemie, eine Darstellung der Chemie der Kolloide und verwandter Gebiete, Akademische Verlagsgesellschaft, 1909.
[52] J.A. DeMessie, G.A. Sorial, E. Sahle-Demessie, Removing chromium (VI) from contaminated water using a nano-chitosan–coated diatomaceous earth, in: S. Ahuja (Ed.), Separations of Water Pollutants with Nanotechnology, vol. 15, Academic Press, Cambridge, 2022, pp. 163–176, https://doi.org/10.1016/B978-0-323-90763-7.00005-6.
[53] S.V. Mohan, J. Karthikeyan, Removal of lignin and tannin colour from aqueous solution by adsorption onto activated charcoal, Environ. Pollut. 97 (1997) 183–187, https://doi.org/10.1016/S0269-7491(97)00025-0.
[54] J. Lyklema, Adsorption at the Solid-Gas Interface in Fundamentals of Interface and Colloid Science, vol. 2, Academic Press, 1995, https://doi.org/10.1016/S1874-5679(06)80004-8, 1-1-1-118, ISSN 1874-5679, ISBN 9780124605244.
[55] S. Brunauer, , P. H. Emmett, E. Teller, Adsorption of gases in multimolecular layers, J. Am. Chem. Soc. 60 (2) 309-319. doi:10.1021/ja01269a023. ISSN 0002-7863..
[56] N. Gupta, A.K. Kushwaha, M.C. Chattopadhyaya, Adsorptive removal of Pb2+, Co2 + and Ni2+ by hydroxyapatite/chitosan composite from aqueous solution,

J. Taiwan Inst. Chem. Eng. 43 (2012) 125–131, https://doi.org/10.1016/j.jtice.2011.07.009.
[57] Y.J. Lee, E.J. Elzinga, R.J. Reeder, Sorption mechanisms of zinc on hydroxyapatite: systematic uptake studies and EXAFS spectroscopy analysis, Environ. Sci. Technol. 39 (2005) 4042–4048, https://doi.org/10.1021/es048593r.
[58] X. Cao, L.Q. Ma, D.R. Rhue, C.S. Appel, Mechanisms of lead, copper, and zinc retention by phosphate rock, Environ. Pollut. 131 (2004) 435–444, https://doi.org/10.1016/j.envpol.2004.03.003.
[59] T. Suzuki, K. Ishigaki, M. Miyake, Synthetic hydroxyapatites as inorganic cation exchangers. Part 3.—exchange characteristics of lead ions (Pb 2+), J. Chem. Soc. Faraday Trans. I 80 (1984) 3157–3165, https://doi.org/10.1039/F19848003157.
[60] J. Santillan-Medrano, J.J. Jurinak, The chemistry of lead and cadmium in soil: solid phase formation, J. Chem. Soc. Faraday Trans. I 39 (1975) 851–856, https://doi.org/10.2136/sssaj1975.03615995003900050020x.
[61] C.K. Lewicke, Treating lead and fluoride wastes, Environ. Sci. Technol. 6 (1972) 321–322.
[62] J.O. Nriagu, Lead orthophosphates, IV. Formation and stability in the environment, Geochem. Cosmochim. Acta 38 (1974) 887–898, https://doi.org/10.1016/0016-7037(74)90062-3.
[63] T. Suzuki, T. Hatsushika, Y. Hayakawa, Synthetic hydroxyapatites employed as inorganic cation exchangers, J. Chem. Soc. Faraday Trans. I 77 (1981) 1059–1062, https://doi.org/10.1039/F19817701059.
[64] T. Suzuki, T. Hatsushika, M. Miyake, Synthetic hydroxyapatites as inorganic cation exchangers, Part 2, J. Chem. Soc. Faraday Trans. I 78 (1982) 3605–3611, https://doi.org/10.1039/F19827803605.
[65] J. Santillan-Medrano, J.J. Jurinak, The chemistry of lead and cadmium in soil: solid phase formation, J. Chem. Soc. Faraday Trans. I 39 (1975) 851–856, https://doi.org/10.2136/sssaj1975.03615995003900050020x.
[66] J.O. Nriagu, Formation and stability of base metal phosphates in soils and sediments, in: J.O. Nriagu, P.B. Moore (Eds.), Phosphate Minerals, Springer, Berlin, 1984, pp. 318–329, https://doi.org/10.1007/978-3-642-61736-2_10.
[67] Y. Xu, F.W. Schwartz, Lead immobilization by hydroxyapatite in aqueous solutions, J. Contam. Hydrol. 15 (1994) 187–206, https://doi.org/10.1016/0169-7722(94)90024-8.
[68] Y. Takeuchi, H. Arai, Removal of coexisting Pb^{2+}, Cu^{2+} and Cd^{2+} ions from water by addition of hydroxyapatite powder, J. Chem. Eng. Jpn. 23 (1990) 75–80, https://doi.org/10.1252/jcej.23.75.
[69] J.E. McLean, B.E. Bledsoe, Behavior of Metals in Soils, Environ. Prot. Agency Ground Water, 1992. Iss EPA/540/s-92/018.
[70] P.B. Tchounwou, C.G. Yedjou, D.N. Foxx, A.B. Ishaque, E. Shen, Lead-induced cytotoxicity and transcriptional activation of stress genes in human liver carcinoma (HepG 2) cells, Mol. Cell. Biochem. 255 (2004) 161–170, https://doi.org/10.1023/b:mcbi.0000007272.46923.12.
[71] Agency for Toxic Substances and Disease Registry (ATSDR), Toxicological Profile for Lead; Public Health Service, U.S. Department of Health and Human Services, Atlanta, GA, USA, 1999.
[72] J.L. Pirkle, R.B. Kaufmann, D.J. Brody, T. Hickman, E.W. Gunter, D.C. Paschal, Exposure of the US population to lead, 1991-1994, Environ. Health Perspect. 106 (1998) 745–750, https://doi.org/10.1289/ehp.98106745.
[73] K.G. Li, J.T. Chen, S.S. Bai, X. Wen, S.Y. Song, Q. Yu, J. Li, Y.Q. Wang, Intracellular oxidative stress and cadmium ions release induce cytotoxicity of unmodified cadmium sulfide quantum dots, Toxicol. Vitro 23 (2009) 1007–1013, https://doi.org/10.1016/j.tiv.2009.06.020.
[74] H. Oubrahim, E.R. Stadtman, P.B. Chock, Mitochondria play no roles in Mn (II)-induced apoptosis in HeLa cells, Proc. Natl. Acad. Sci. USA 98 (2001) 9505–9510, https://doi.org/10.1073/pnas.181319898.
[75] Y. Škreb, V. Habazin-Novak, N. Horš, The rate of DNA synthesis in Hela cells during combined long-term and acute exposures to lead, Toxicology 19 (1981) 1–10, https://doi.org/10.1016/0300-483x(81)90059-7.
[76] M.M. Mumtaz, D.B. Tully, H.A. El-Masri, C.T. De Rosa, Gene induction studies and toxicity of chemical mixtures, Environ. Health Perspect. 110 (2002) 947–956, https://doi.org/10.1289/ehp.02110s6947.
[77] M. Abdullah, F.A. Rahman, N. Gnanasegaran, V. Govindasamy, N.H. Abu Kasim, S. Musa, Diverse effects of lead nitrate on the proliferation, differentiation, and gene expression of stem cells isolated from a dental origin, Sci. World J. 2014 (2014) 1–11, https://doi.org/10.1155/2014/235941.
[78] A. Hartwig, R. Schlepegrell, D. Beyersmann, Indirect mechanism of lead-induced genotoxicity in cultured mammalian cells, Mutat. Res. Genet. Toxicol. 241 (1990) 75–82, https://doi.org/10.1016/0165-1218(90)90110-N.